npj | computational materials

Article

Published in partnership with the Shanghai Institute of Ceramics of the Chinese Academy of Sciences

https://doi.org/10.1038/s41524-026-02040-x

Prediction of ambient-pressure high-temperature superconductivity in electronically modified transition-metal hydrides

Haowei Xu[1,2] ✉, Olivia Schneble[3], Rafael Jaramillo[3], Marek Polański[4] & Ju Li[2,3] ✉

The search for conventional superconductors with high transition temperatures (T_c) has largely focused on intrinsically metallic compounds. In this work, we explore the potential of intrinsically *non-metallic* compounds to exhibit high-T_c superconductivity under ambient pressure through carrier doping. We identify $MgAlFeH_6$, a representative of carrier-doped transition-metal hydrides like Mg_2FeH_6, as a promising example with a predicted $T_c \approx 130$ K. We propose that the *average projected electron density of states* (DOS), defined as the geometric mean of the total and hydrogen-projected DOS at the Fermi level, serves as a simple and computationally inexpensive indicator of high-T_c behavior. Notably, the correlation between T_c and the average projected DOS is stronger than that between T_c and either total DOS or hydrogen-projected DOS. We also highlight the tradeoff between high-T_c and dynamic stability, both of which depend on the electron DOS at the Fermi level. Our findings thus expand the pool of potential superconducting materials and offer a practical route for accelerating the discovery of superconductors suitable for real-world applications.

Since the discovery of superconductivity in mercury in 1911, researchers have persistently sought materials with superconducting transition temperatures T_c above room temperature ($\approx$ 300 K), or at least above the temperature of liquid nitrogen ($\approx$ 77 K). While the latter have been achieved in a class of cuprate compounds[1,2], their underlying physical mechanism remains elusive. In contrast, the mechanism of so-called conventional superconductivity is well established through the BCS theory[3,4], where phonons are responsible for electron pairing. For decades, the T_c of conventional superconductors remains far below the temperature of liquid nitrogen. This changed with the advent of hydride compounds, particularly H_3S, which demonstrates a T_c of around 200 K in both ab initio calculations and experiments[5–7]. Furthermore, several other hydrides, including YH_6[8], CaH_6[9], and LaH_{10}[10–12], have also been proposed to have high T_c.

Unfortunately, the hydride compounds mentioned above are dynamically stable only under extremely high pressures (typically exceeding 100 GPa), severely limiting their practical applicability. In this regard, recent research efforts have focused on discovering high-T_c hydrides that can be stable under ambient pressure[13,14]. Particularly, refs. 15,16. predicted that a class of materials, Mg_2XH_6 with X = Rh, Ir, Pd, or Pt, could exhibit T_c reaching 100 K at ambient pressure. From a practical perspective, however, these exciting results are undermined by the fact that Rh, Ir, Pd, and Pt are all noble metals with prices comparable to, or even higher than, that of gold.

Clearly, it is a grand challenge to identify superconductors suitable for practical applications, namely those with (i) low-cost, (ii) stability at ambient pressure, and (iii) high-T_c above liquid nitrogen temperature or even room temperature. Actually, despite the vastness of the known materials database, which contains millions of entries[17,18], it is uncertain whether such materials really exist within it. Notably, most previous studies have focused on intrinsically metallic materials, which limits the pool of candidates in materials genome searches. However, semiconductors and even insulators can have metallic behavior and exhibit superconductivity under certain conditions, such as carrier doping. Two prominent examples are the prototypical unconventional superconductor $YBa_2Cu_3O_{7-\delta}$ (YBCO), which is a Mott insulator in its undoped state ($\delta \approx 1$)[1,19]; and boron-doped diamond, which becomes superconducting ($T_c \approx 4$K) with sufficient boron dopants[20]. These findings motivate us to explore the potential of *non-metallic* materials as superconductors. Indeed, multi-component hydrides can exist as stoichiometric compounds, and it is also easy to partially

[1]Department of Physics, City University of Hong Kong, Kowloon, Hong Kong SAR, China. [2]Department of Nuclear Science and Engineering, Massachusetts Institute of Technology, Cambridge, MA, USA. [3]Department of Materials Science and Engineering, Massachusetts Institute of Technology, Cambridge, MA, USA. [4]Military University of Technology, Warsaw, Poland. ✉e-mail: haoweixu@cityu.edu.hk; liju@mit.edu

substitute[21,22] elements, changing the thermodynamic properties while keeping the crystal structure.

In this work, we use ternary or quaternary transition-metal hydrides[23] as an example to demonstrate the potential of electronically modified semiconductor/insulators as high-T_c superconductors at ambient pressure. Instead of using brute-force high-throughput calculations, we adopt a rational materials design approach. We begin with non-metallic transition-metal hydrides as identified in ref. 23 and focus on compounds that exhibit van Hove singularities in the *average projected electronic density of states* (DOS) near the valence band maximum (VBM) or conduction band minimum (CBM). As we will show later, the average projected electron DOS, which is defined as the geometric average of the total DOS and the hydrogen-projected DOS, shows a strong correlation with T_c. We argue that it can serve as an easy-to-compute indicator of potentially high superconducting critical temperatures. Carrier doping is then introduced through atomic substitution, insertion, or removal. The dynamic stability of the doped structures is assessed via their phonon band structures. For dynamically stable systems, we proceed to calculate their T_c. Our search is restricted to candidates with fewer than ~20 atoms per unit cell, which are tractable for ab initio T_c calculations. Using this approach, we identify Mg_2FeH_6 as a promising platform for high-T_c superconductivity at ambient pressure under carrier doping. Note that Mg_2FeH_6 has been synthesized before[24–26] by reactive mechanical alloying in a hydrogen atmosphere, and by high-temperature solid-state reaction. In particular, we find that the electron-doped variant, $MgAlFeH_6$, exhibits a predicted T_c of up to 130 K. Additionally, we highlight the critical interplay between high T_c and dynamic stability, both of which can arise from a high electron DOS near the Fermi level. Our methodology, which emphasizes carrier doping in non-metallic systems, is not limited to transition-metal hydrides like Mg_2FeH_6. It can be broadly applied to expand the superconducting materials search space and potentially accelerate the discovery of compounds suitable for practical applications.

In the following, we first present the atomic structures, phonon spectra, and electronic properties of Mg_2FeH_6 and its electron- and hole-doped variants, $MgAlFeH_6$ and $MgNaFeH_6$. We find that $MgAlFeH_6$ is dynamically stable and thermodynamically metastable with an energy above hull of around 0.11 eV per atom. In contrast, $MgNaFeH_6$ is dynamically unstable. We attribute this behavior to the exceptionally high electron DOS near the Fermi level in the latter. We then analyze the electron-phonon coupling and superconducting properties of $MgAlFeH_6$, highlighting a predicted T_c of ~130 K. Finally, we explore the effect of charge doping on superconductivity in Mg_2FeH_6 in a more general context, demonstrating that T_c up to 100 K can also be achieved. We also underscore a strong correlation between T_c and the average projected electron DOS in doped Mg_2FeH_6.

Results

Phonon structures and stability of $MgAlFeH_6$

Pristine Mg_2FeH_6 is a non-magnetic band insulator with a bandgap of around 2 eV, according to our density functional theory (DFT) calculations. It thus cannot be a superconductor in its intrinsic state. Nevertheless, the electron DOS of Mg_2FeH_6 features two van Hove peaks near VBM and CBM. This property, together with the high-frequency phonons resulting from H atoms, suggests the potential of high T_c in Mg_2FeH_6, provided that the electron Fermi level can be shifted into either the valence or the conduction bands. While this can be achieved by multiple strategies, such as removing or adding H atoms, we will focus on the effect of substituting Mg with Al (electron doping) or Na (hole doping) in this work. For now, we will explore the properties of $MgAlFeH_6$ ($MgNaFeH_6$) with an ordered lattice structure, that is, one of the two Mg atoms in the primitive cell is replaced by Al (Na). This is to keep the unit cell small (9 atoms), so that ab initio calculations on T_c can be tractable. Later, we will discuss how the electric properties of doped Mg_2FeH_6 depend on the carrier concentration under more general settings.

We begin by analyzing the atomic structure and dynamic stability of the Al/Na-substituted systems. Pristine Mg_2FeH_6 has a cubic structure with space group $Fm\bar{3}m$ (no. 225), which is reduced to $F\bar{4}3m$ (no. 216) after one of the two Mg atoms is replaced by Al or Na (inset of Fig. 1a). Our DFT calculations indicate that $MgAlFeH_6$ tends to retain such a high symmetry structure, even if small perturbations are added to the initial structure before DFT relaxations. The lattice constant of $MgAlFeH_6$ is around 6.24 Å. Mg, Al, and Fe atoms occupy the 4*d* (0.75, 0.75, 0.75), 4*c* (0.25, 0.25, 0.25), and 4*b* (0.5, 0.5, 0.5) positions, respectively, while H atoms occupy the 24*f* (0.24, 0, 0) Wyckoff positions. The phonon dispersions and projected phonon DOS of Mg_2FeH_6 and $MgAlFeH_6$ are plotted in Fig. 1a, b, showing similar characteristics. No imaginary frequencies are found over the whole Brillouin zone, indicating their dynamic stability. The low-frequency branches ($\lesssim$10 THz) are mostly contributed by the metal atoms, while the high-frequency branches (10 ~ 60 THz) are dominated by H atoms. The phonons of $MgAlFeH_6$ are slightly softened compared to Mg_2FeH_6. Moreover, the dynamical stability of $MgAlFeH_6$ is also verified by anharmonic phonon calculations using the stochastic self-consistent harmonic approximation (SSCHA)[27–32], as well as molecular dynamics simulations at 300 K [Supplementary Figs. S3, S4]. In contrast, $MgNaAlH_6$ turns out to be dynamically unstable, as its phonon dispersion exhibits imaginary frequencies over almost the entire Brillouin zone (Fig. 1c). We will return to this point later.

Thermodynamically, $MgAlFeH_6$ is a meta-stable state. The formation energy of the reaction $Mg + Al + Fe + 3H_2 \rightarrow MgAlFeH_6$ is around -0.10 eV per atom. This should be compared with the formation energy of Mg_2FeH_6 (i.e., $2Mg + Fe + 3H_2 \rightarrow Mg_2FeH_6$), which is around -0.06 eV per atom. In this sense, the formation of $MgAlFeH_6$ should be feasible. However, there exists a competing reaction path when Mg, Al, Fe, and H_2 are mixed, namely $6Mg + 6Al + 6Fe + 17H_2 \rightarrow 5AlH_3 + 3Mg_2FeH_6 + AlFe_3H$, whose formation energy is around -0.21 eV per atom. In other words, $MgAlFeH_6$ is only metastable, as it has a decomposition pathway $6MgAlFeH_6 \rightarrow 5AlH_3 + 3Mg_2FeH_6 + AlFe_3H + H_2$. The corresponding decomposition energy is around 0.11 eV per atom. Nevertheless, $MgAlFeH_6$ may still be synthesizable. While an energy above the convex hull of around 0.1 eV per atom is often used as a practical criterion for "synthesizable" compounds, many materials with substantially higher energies above the hull have been successfully realized[33]. A notable example is the promising superconductor PdH_3, with an energy above the convex hull of ~0.144 eV per atom (at 30 GPa). PdH_3 has recently been synthesized[34]. Another well-known example is diamond, whose energy is around 0.13 eV per atom above that of graphite. Furthermore, as indicated by our molecular dynamics and anharmonic phonon simulations (Supplementary Figs. S3, S4), $MgAlFeH_6$ is dynamically stable even at 300 K. Therefore, the *as-synthesized* $MgAlFeH_6$ is unlikely to undergo a solid-state phase transition or decompose easily, which requires the separation of Al and Fe. Hence, the primary experimental challenge may lie in the synthesis of $MgAlFeH_6$ itself. Increasing the H_2 pressure can favor this pathway by suppressing the competing reactions. More generally, high-pressure synthesis may be advantageous, as exemplified by diamond and many other hydrogen-rich superconductors. Meanwhile, as we will elaborate later, an ordered lattice of $MgAlFeH_6$ is not required for our purpose; in principle, the introduction of Al atoms serves only to provide free carriers in the system. This consideration offers some flexibility in the synthesis of the compound. For example, Al ion implantation might be employed to substitute Mg atoms in Mg_2FeH_6.

Electronic structure and van Hove singularities in MgAlFeH6

The electronic structures of $MgAlFeH_6$ and $MgNaFeH_6$ are plotted in Fig. 1d, e, respectively. In contrast to Mg_2FeH_6, which has a bandgap of around 2 eV, the Fermi level of $MgAlFeH_6$ lies in the conduction band and is very close to the van Hove peak in the total electron DOS. Furthermore, the projected electron DOS indicates that H atoms have significant contributions to the total DOS, and the Fermi level is also close to the peak of the H-projected DOS. This suggests that when H atoms are displaced upon phonon excitation, the electronic structure may be significantly altered, potentially leading to strong electron-phonon coupling and high T_c.

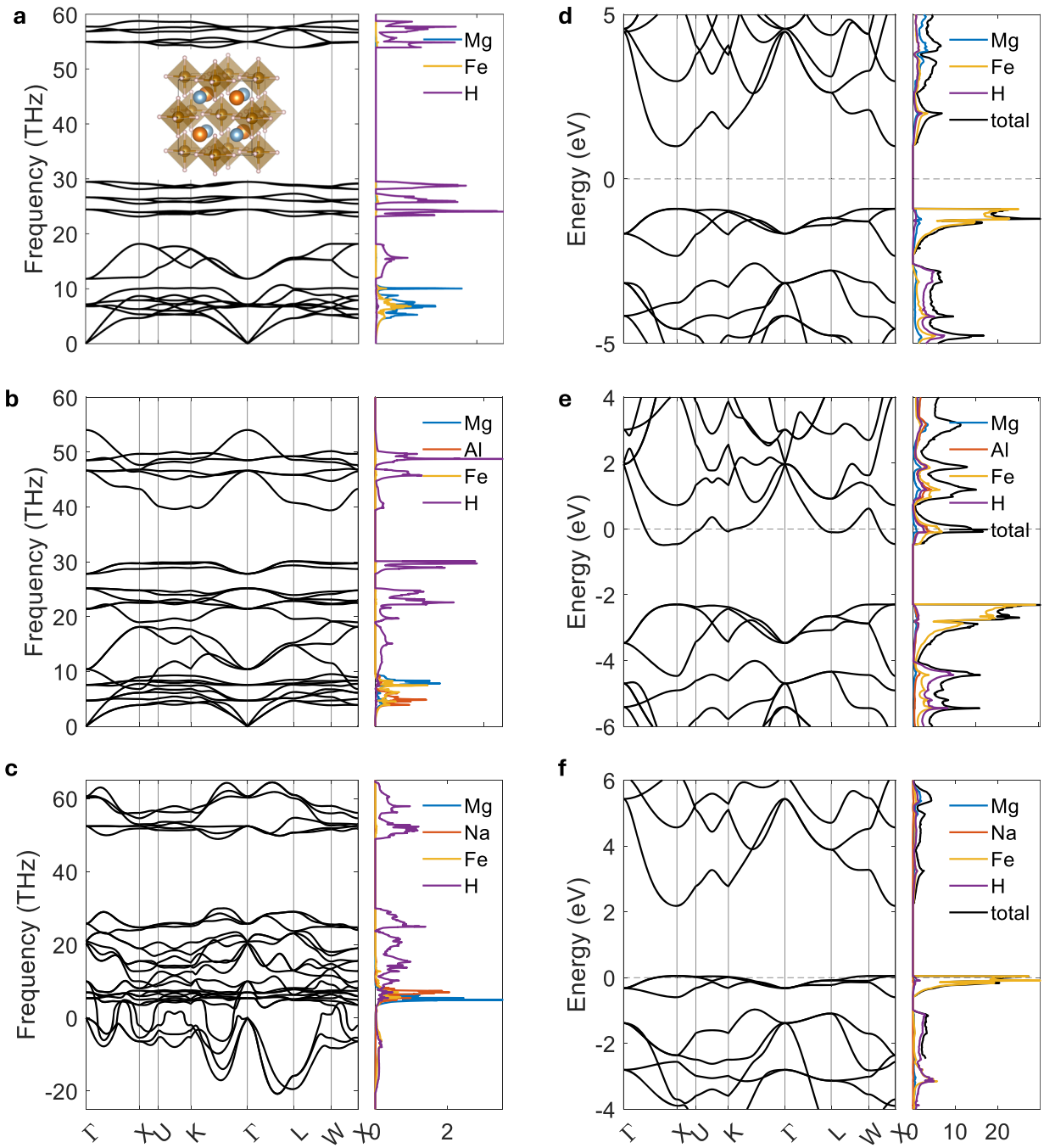

Fig. 1 | Electronic and phonon structures of Mg_2FeH_6, $MgAlFeH_6$, and $MgNaFeH_6$. Phonon structure of **a** Mg_2FeH_6, **b** $MgAlFeH_6$, and **c** $MgNaFeH_6$. The phonon dispersion on high-symmetry lines in the Brillouin zone is plotted on the left-hand side, while the projected phonon DOS is plotted on the right-hand side. Mg_2FeH_6 and $MgAlFeH_6$ exhibit dynamic stability, while $MgNaFeH_6$ is dynamically unstable with imaginary frequency phonons spanning almost the entire Brillouin zone. **d**–**f**, same as (**a**–**c**), but for electronic structures. The energy is offset to the electron Fermi level for each compound. The phonon (electron) DOS has the units of states per THz (eV) per formula unit. Inset of (**a**): Atomic structure $MgAlFeH_6$ with an ordered lattice. Brown: Fe; orange: Mg; cyan: Al; pink: H. In pristine Mg_2FeH_6, both Mg and Al sites are occupied by Mg atoms.

On the other hand, the Fermi level of $MgNaFeH_6$ lies in the valence band and is close to an even more pronounced van Hove peak (Fig. 1f), as the conduction bands are rather flat. Such an extremely high electron DOS at the Fermi level may be the reason why $MgNaFeH_6$ is dynamically unstable – the sharp and pronounced van Hove peak makes the electronic structure highly sensitive to atomic displacements[35]. This may enhance electron-phonon interactions, which could favor a high T_c. However, the same mechanism also implies structural instability, as small perturbations may lead to drastic changes in the electronic properties, potentially destabilizing the system. This is indeed observed in the phonon band structure of $MgNaFeH_6$, as we discussed before. This highlights the critical tradeoff between high T_c and dynamic stability in designing conventional (and potentially even unconventional) superconductors – both properties depend on the electron DOS near the Fermi level. While a high electron DOS enhances superconducting pairing, it may also destabilize the lattice, presenting a key challenge in materials optimization.

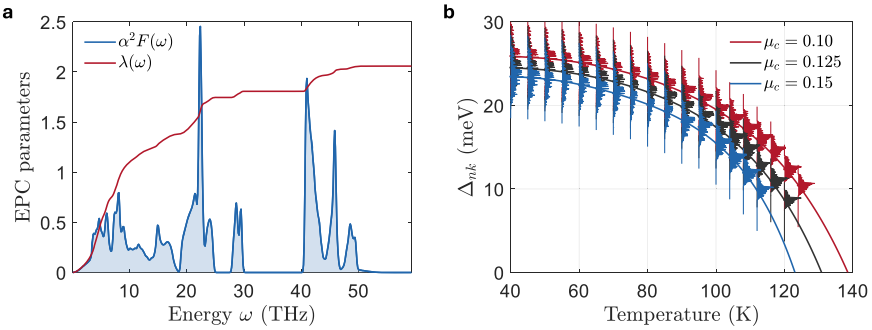

Fig. 2 | Electron-phonon coupling and superconductivity of $MgAlFeH_6$. **a** Eliashberg spectral function $\alpha^2F(\omega)$ and accumulated electron-phonon coupling $\lambda(\omega)$. The EPC constant is $\lambda(\omega \to \infty) \approx 2.1$. The effective Colomb potential is set to $\mu_c = 0.1$ for this plot. **b** Histograms of the distribution of the anisotropic superconducting gap Δ_{nk} as a function of energy, which are obtained by solving the anisotropic Eliashberg equation at different temperatures T. Three different $\mu_c =$ 0.1, 0.125, and 0.15 are used. The solid lines fit the average of Δ_{nk} at each temperature, which are then extrapolated to yield the superconducting transition temperature T_c.

Superconductivity in MgAlFeH6

Next, we demonstrate the electron-phonon and superconducting properties in $MgAlFeH_6$. The Eliashberg spectral function $\alpha^2F(\omega)$ and the cumulative electron-phonon coupling (EPC) parameter $\lambda(\omega) = 2\int_0^{\omega} \frac{\alpha^2F(\omega)}{\omega} d\omega$ are plotted in Fig. 2a. The EPC constant $\lambda \equiv \lambda(\infty)$ is as large as 2.1, comparable to that of H_3S at 200 GPa[5–7]. To obtain the superconducting transition temperature T_c, we solve the anisotropic Eliashberg equations on the imaginary-axis and then continue to the real-axis by Padé approximation[36,37]. The histograms of the distribution of the anisotropic superconducting gap Δ_{nk} is plotted in Fig. 2b as a function of temperature T. The effective Coulomb potential μ_c in this calculation is an empirical parameter, which represents the repulsive electron-electron interaction. We used several different $\mu_c = 0.1,\ 0.125$, and 0.15, which are typical values for conventional superconductors. By extrapolating the $\Delta_{nk}(T)$ curves to $\Delta_{nk}(T_c) = 0$, we obtain $T_c \approx 130$ K.

The above discussions assumed an ordered lattice of $MgAlFeH_6$. In practice, depending on the synthesis approach, Mg and Al atoms may randomly occupy the original sites of Mg atoms in pristine Mg_2FeH_6. To account for this effect, we constructed a supercell $Mg_{32}Al_{32}Fe_{32}H_{192}$ with 288 atoms in total. Here, 32 Mg and 32 Al atoms are randomly placed, representing a random alloy. The electronic and phonon properties of this supercell are shown in Fig. 3. This structure is dynamically stable with no imaginary frequency phonons (Supplementary Fig. S1). Compared with ordered $MgAlFeH_6$, the electron and phonon DOS are smeared out due to inhomogeneity. Nevertheless, some characteristic features that prelude high T_c remain, including high total and H-projected electron DOS, as well as the high frequency of phonon vibrations. Hence, a relatively high T_c could be expected, though a precise calculation of T_c of this supercell is not possible due to the formidable computational cost. Nevertheless, we can use the *average projected electron DOS*, which we will elaborate on below, as an indicator of T_c. The T_c of the random alloy is estimated to be around 40 K. This is significantly lower than the of the ordered lattice (above 100 K), as the van Hove singularity in electron DOS is broadened in the random alloy. It is also worth noting that according to P. W. Anderson[38], superconductivity in a conventional superconductor is robust with respect to non-magnetic disorder in the host material, provided the disorder is not too strong – for example, near a superconductor-insulator transition. Indeed, highly disordered structures, including Ta-Nb-Hf-Zr-Ti high-entropy alloy, can exhibit T_c of up to 10 K[39,40]. It is thus highly interesting to experimentally explore the potential of a random-alloy phase of $MgAlFeH_6$ for achieving a higher T_c.

As previously mentioned, substituting Mg with Al is just one of several possible strategies for inducing superconductivity in Mg_2FeH_6. Particularly, $MgAlFeH_6$ is an alloy of the parent compound Mg_2FeH_6 with high carrier concentration, but the core concept can be seen at lower carrier concentrations, down towards the regime of doping. In principle, any method that introduces free carriers could be effective. To explore these strategies in a more general way, we directly vary the total number of electrons in Mg_2FeH_6 within our DFT calculations. Reducing (increasing) the electron number is equivalent to hole (electron) doping. Note that varying the total number of electrons leads to a divergent Coulomb energy, which can be compensated by adding a uniform background charge of opposite sign in DFT calculations. We adopt this approach to calculate the superconducting critical temperature T_c of charge-doped Mg_2FeH_6 as a function of doping concentration n, where positive and negative values of n (in units of electrons per formula unit, e/f.u., equivalent to 1.6×10^{22}cm^{-3} in the case of Mg_2FeH_6) correspond to hole and electron doping, respectively. When $n \lesssim \pm 0.1\ e$/f.u., the predicted T_c is negligibly small in calculations. This behavior is reminiscent of experimental observations in boron-doped diamond, where the system remains semiconducting below a similar doping threshold[20]. For $n \gtrsim \pm 0.1\ e$/f.u., T_c becomes appreciable and generally increases with doping concentration. At $n \approx \pm 1\ e$/f.u., which is equivalent to the carrier concentrations in $MgAlFeH_6$ and $MgNaFeH_6$, T_c reaches ~100 K, in agreement with the directly calculated T_c for $MgAlFeH_6$. These results support the idea that carrier doping in semiconductors is a viable route to achieving high-T_c superconductivity under ambient conditions. Note that while T_c tends to continue increasing with hole doping concentration $n \gtrsim +1\ e$/f.u., the structure becomes dynamically unstable in this regime, as suggested by the appearance of imaginary-frequency phonon modes in the phonon dispersion (Supplementary Fig. S2). This again highlights the critical tradeoff between high T_c and dynamic stability, both of which depend on the electron DOS. When the electron doping concentration is higher than around $-1.2\ e$/f.u., T_c starts to decrease as the Fermi level is moving away from the van Hove peak in the electron DOS. Note that we model pure carrier doping primarily to demonstrate that high-T_c in doped Mg_2FeH_6 is a relatively generic effect, which is independent of the specific method used to introduce carriers. Achieving pure carrier doping at high concentrations ($0.1 \sim 1\ e$/f.u.), however, may be nontrivial in practice and may only be feasible in, for example, thin-film structures.

Relationship between T_c and average projected electron DOS

Here, a critical observation is that the predicted T_c shows a strong correlation with the average projected electron DOS at the Fermi level, defined as $\bar{D} = \sqrt{D_{\text{total}} D_{\text{H}}}$, where D_{total} and D_{H} are the total and H-projected electron DOS at the Fermi level, respectively. T_c and $\bar{D}$ have almost the same trend as a function of doping concentration (Fig. 4c). This phenomenological correlation can be understood by noting that D_{total} reflects the number of electrons available for superconducting pairing, while D_{H} is closely related to the strength of electron-phonon coupling, which is primarily mediated by H atoms in hydrides. It is worth noting that correlation between T_c and $\bar{D}$ is significantly better than that between T_c and D_{total} or D_{H} individually (Fig. 4a, b).

Compared with phonon and electron-phonon coupling properties, D_{total} and D_{H} are purely electronic quantities that can be efficiently computed from ab initio calculations with relatively low computational cost. As such, $\bar{D}$ may serve as a convenient and practical descriptor for guiding the search for high-T_c superconductivity in both metallic and doped non-metallic hydrides – one can simply look for systems where $\bar{D}$ is maximized at the Fermi level, typically near a van Hove singularity. For compounds lacking hydrogen, $\bar{D}$ can be generalized as $\bar{D} = \sqrt{D_{\text{total}} D_{\text{X}}}$, where X refers to other light atoms, such as boron.

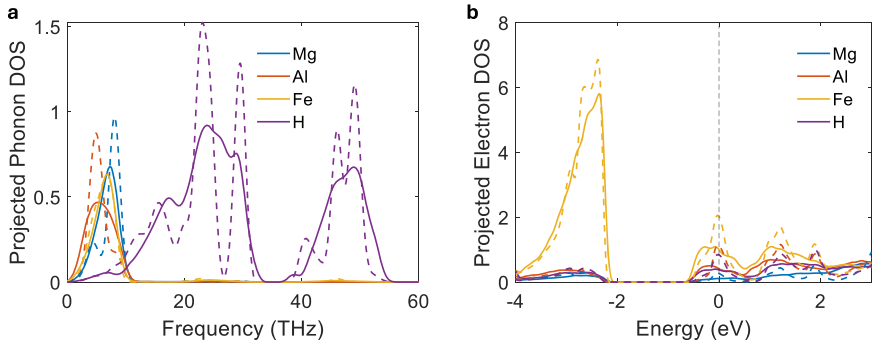

Fig. 3 | Phonon and electronic properties of $MgAlFeH_6$ random alloy. The solid curves are projected (**a**) phonon and (**b**) electron DOS of a $Mg_{32}Al_{32}Fe_{32}H_{192}$ supercell. Mg and Al are randomly placed at the Mg sites in pristine Mg_2FeH_6, representing a random alloy. The dashed curves are results for ordered $MgAlFeH_6$. In (**b**), the energy is offset to the electron Fermi level. The units for the y-axis of (**a**)/(**b**) are states per THz/eV per $MgAlFeH_6$ formula unit.

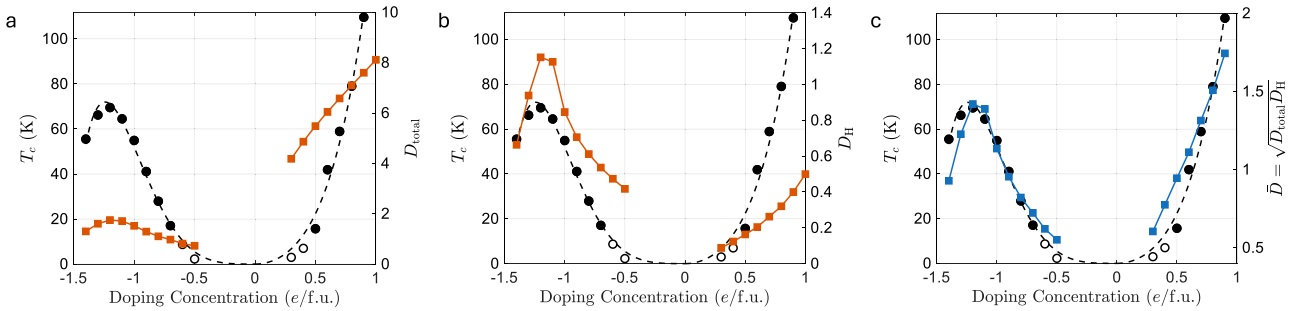

Fig. 4 | Superconductivity transition temperature vs. different types of DOS. Left y-axis: superconducting transition temperature T_c as a function of carrier doping concentration in Mg_2FeH_6. Filled black circles represent values obtained by solving the anisotropic Eliashberg equations, while open black circles are deduced from the Allen-Dynes equation. The dashed black curve serves as a guide to the eye. Right y-axis: various types of electron DOS, including **a** D_{total}, **b** D_{H} and **c** $\bar{D} = \sqrt{D_{\text{total}} D_{\text{H}}}$. The correlation between T_c and $\bar{D}$ is significantly better than that between T_c and D_{total} or D_{H}. The electron density of states is in the unit of states per eV per formula unit.

Discussion

From an experimental perspective, electron- and hole-doping may be achieved electrically, electrochemically, or chemically. Electrical doping, or charge doping, can be achieved by applying an electric field or by creating a heterojunction, in which a local space charge is induced. Such controllable and localized (nearly 2D) superconductivity may be of interest for numerous applications in information processing or sensing. The 3D substrate may also provide a mechanical constraint to prevent phase transformation that may otherwise happen. To carry a lot of current, however, requires 3D superconductors, and this may be achieved by electrochemical hydrogenation[41], chemical hydrogenation, chemical alloying, or chemical substitution, where electroneutrality is satisfied in the bulk. Generally speaking, electron (hole) doping corresponds to decreasing (increasing) the electrochemical voltage U or going to more "reducing" ("oxidative") local chemical conditions, by e.g., increasing (decreasing) the hydrogen partial pressure P_{H2}, as the typical Brouwer diagram of semiconducting oxide shows. We note that while $MgAlFeH_6$, $MgNaFeH_6$, etc. appear to have unusual valences, such exotic-valence compounds do exist in nature. Examples include high-voltage cathode oxide particles inside lithium-ion batteries[42] or zirconium suboxide in metallic zirconium oxidation[43]. Achieving these compounds by creating very reducing or oxidative local conditions – either thermodynamically or kinetically[44,45] – may still be experimentally more feasible than applying the hundreds of GPa mechanical pressure required for many high-T_c hydrides like H_3S.

In summary, we demonstrate that Mg_2FeH_6, an intrinsic semiconductor, can be transformed into an ambient-pressure superconductor with T_c above 100 K through electronic modification, such as carrier doping. Unlike most previous studies that have focused on intrinsically metallic compounds, our work highlights the potential of non-metallic systems as promising platforms for high-temperature superconductivity upon electronic modification, thereby broadening the pool of candidate materials. Furthermore, we identify the average projected electron density of states as an easy-to-compute genome that can accelerate the discovery of high-T_c superconductors. Future work applying these methodologies may lead to the discovery of additional superconductors suitable for practical applications.

Methods

Ab initio calculations

The first-principles calculations in this work are based on density functional theory (DFT)[46,47] using the Quantum Espresso package[48,49]. The PBEsol[50,51] exchange-correlation functional is adopted. Core and valence electrons are treated with the projected augmented wave (PAW) method[52] and plane wave basis, respectively. The atomic structures, as well as the lattice constants, are relaxed until the forces on each other are smaller than 10^{-3} eV/A. We used $17 \times 17 \times 17$ k-mesh in the relaxation step. The kinetic energy cutoff is set to 60 Ry. Electronic Hamiltonians in the Wannier basis are then built from plane-wave DFT results, using the Wannier90 package[53]. The s-orbital of H, d-orbital of Fe, and p-orbital of Mg and Al are used in the Wannierization process. The electron-phonon coupling and superconductivity properties are calculated with the help of the EPW package[54,55]. To compute the superconducting transition temperature, $5 \times 5 \times 5$ coarse (before Wannier interpolation) and $25 \times 25 \times 25$ fine (after Wannier interpolation) meshes are used to sample the first Brillouin zone of both electrons and phonons. The anharmonic phonon calculations using the stochastic self-consistent harmonic approximation (SSCHA) are performed using the SSCHA package[27,28]. For SSCHA calculations, we used a $3 \times 3 \times 3$ super cell with 243 atoms in total. The supercell is greater than 10 A along each dimension. We used auxiliary phonon calculations, and 50 structural configurations were used to converge the phonons. The molecular dynamics simulations are performed using a Langevin thermostat with a timestep of 1 fs.

Data availability

The datasets generated and/or analyzed during the current study are not publicly available, as the primary data supporting the findings are contained within the main text and the supplementary information files. Further detailed data is available from the corresponding author on reasonable request.

Received: 15 December 2025; Accepted: 7 March 2026;
Published online: 28 March 2026

References

1. Bednorz, J. G. & Müller, K. A. Possible highTc superconductivity in the Ba−La−Cu−O system. *Z. Phys. B Condens. Matter* **64**, 189 (1986).
2. Bednorz, J. G. & Müller, K. A. Perovskite-type oxides–the new approach to high-T_c superconductivity. *Rev. Mod. Phys.* **60**, 585 (1988).
3. Bardeen, J., Cooper, L. N. & Schrieffer, J. R. Microscopic theory of superconductivity. *Phys. Rev.* **106**, 162 (1957).
4. Bardeen, J., Cooper, L. N. & Schrieffer, J. R. Theory of superconductivity. *Phys. Rev.* **108**, 1175 (1957).
5. Li, Y., Hao, J., Liu, H., Li, Y. & Ma, Y. The metallization and superconductivity of dense hydrogen sulfide. *J. Chem. Phys.* **140**, 174712 (2014).
6. Duan, D. et al. Pressure-induced metallization of dense (H2S)2H2 with high-Tc superconductivity. *Sci. Rep.* **4**, 6968 (2014).
7. Drozdov, A. P., Eremets, M. I., Troyan, I. A., Ksenofontov, V. & Shylin, S. I. Conventional superconductivity at 203 kelvin at high pressures in the sulfur hydride system. *Nature* **525**, 73 (2015).
8. Li, Y. et al. Pressure-stabilized superconductive yttrium hydrides. *Sci. Rep.* **5**, 9948 (2015).
9. Wang, H., Tse, J. S., Tanaka, K., Iitaka, T. & Ma, Y. Superconductive sodalite-like clathrate calcium hydride at high pressures. *Proc. Natl. Acad. Sci.* **109**, 6463–6466 (2012).
10. Somayazulu, M. et al. Evidence for superconductivity above 260 K in lanthanum superhydride at megabar pressures. *Phys. Rev. Lett.* **122**, 027001 (2019).
11. Drozdov, A. P. et al. Superconductivity at 250 K in lanthanum hydride under high pressures. *Nature* **569**, 528 (2019).
12. Errea, I. et al. Quantum crystal structure in the 250-kelvin superconducting lanthanum hydride. *Nature* **578**, 66 (2020).
13. He, Y., Lu, J., Wang, X. & Shi, J. Phonon-mediated superconductivity in the metal-bonded perovskite Al_4 H up to 54 K under ambient pressure. *Phys. Rev. B* **108**, 054515 (2023).
14. He, Y. & Shi, J.-J. Few-hydrogen high-Tc superconductivity in (Be4) 2H nanosuperlattice with promising ductility under ambient pressure. *Nano Lett.* **23**, 8126 (2023).
15. Sanna, A. et al. Prediction of ambient pressure conventional superconductivity above 80 K in hydride compounds. *Npj Comput Mater.* **10**, 44 (2024).
16. Dolui, K. et al. Feasible route to high-temperature ambient-pressure hydride superconductivity. *Phys. Rev. Lett.* **132**, 166001 (2024).
17. Zagorac, D., Müller, H., Ruehl, S., Zagorac, J. & Rehme, S. (IUCr) Recent developments in the inorganic crystal structure database: theoretical crystal structure data and related features. *J. Appl. Crystallogr.* **52**, 918–925 (2019).
18. Jain A. et al. Commentary: The Materials Project: a materials genome approach to accelerating materials innovation. *APL Mater.* **1**, 011002 (2013).
19. Lee, P. A., Nagaosa, N. & Wen, X. G. Doping a Mott insulator: Physics of high-temperature superconductivity. *Rev. Mod. Phys.* **78**, 17–85 (2006).
20. Ekimov, E. A. et al. Superconductivity in diamond. *Nature* **428**, 542–545 (2004).
21. Pericoli, E. et al. Synthesis and hydrogen storage properties of Mg-based complex hydrides with multiple transition metal elements. *ACS Appl. Energy Mater.* **8**, 4993–5003 (2025).
22. Rzeszotarska, M., Dworecka-Wójcik, J., Dębski, A., Czujko, T. & Polański, M. Magnesium-based complex hydride mixtures synthesized from stainless steel and magnesium hydride with subambient temperature hydrogen absorption capability. *J. Alloy. Compd.* **901**, 163489 (2022).
23. Yvon, K. & Guillaume, R. Hydrides: solid state transition metal complexes. *Encycl. Inorg. Chem*. https://doi.org/10.1002/0470862106.ia087 (2006).
24. Sai Raman, S. S., Davidson, D. J., Bobet, J.-L. & Srivastava, O. N. Investigations on the synthesis, structural and microstructural characterizations of Mg-based K2PtCl6 type (Mg2FeH6) hydrogen storage material prepared by mechanical alloying. *J. Alloy. Compd.* **333**, 282 (2002).
25. Retuerto, M. et al. Neutron powder diffraction, x-ray absorption and Mössbauer spectroscopy on Mg2FeH6. *Int. J. Hydrog. Energy* **40**, 9306 (2015).
26. Didisheim, J. J. et al. Dimagnesium iron(II) hydride, Mg2FeH6, containing octahedral FeH64- anions. *Inorg. Chem.* **23.13**, 1953–1957 (1984).
27. Errea, I. First-principles theory of anharmonicity and the inverse isotope effect in superconducting palladium-hydride compounds. *Phys. Rev. Lett.* **111**, 177002 (2013).
28. Monacelli, L. et al. The stochastic self-consistent harmonic approximation: calculating vibrational properties of materials with full quantum and anharmonic effects. *J. Phys. Condens. Matter* **33**, 363001 (2021).
29. Dangić, Đ et al. Ambient pressure high temperature superconductivity in RbPH3 facilitated by ionic anharmonicity. *Comput. Mater. Today* **8**, 100043 (2025).
30. Errea, I. Anharmonic free energies and phonon dispersions from the stochastic self-consistent harmonic approximation: application to platinum and palladium hydrides. *Phys. Rev. B* **89**, 064302 (2014).
31. Bianco, R., Errea, I., Paulatto, L., Calandra, M. & Mauri, F. Second-order structural phase transitions, free energy curvature, and temperature-dependent anharmonic phonons in the self-consistent harmonic approximation: theory and stochastic implementation. *Phys. Rev. B* **96**, 014111 (2017).
32. Monacelli, L., Errea, I., Calandra, M. & Mauri, F. Pressure and stress tensor of complex anharmonic crystals within the stochastic self-consistent harmonic approximation. *Phys. Rev. B* **98**, 024106 (2018).
33. Lee, A. et al. Machine learned synthesizability predictions aided by density functional theory, Commun. *Mater* **3**, 73 (2022).
34. Liu, C. et al. High-Pressure synthesis of metastable superhydride PdH3 by using amorphous Pd as a starting material. *ACS Nano* **19**, 32209–32217 (2025).
35. Yuzbashyan, E. A., Altshuler, B. L. & Patra, A. Instability of metals with respect to strong electron-phonon interaction. *Phys. Rev. Lett.* **135**, 026503 (2025).
36. Verdi, C. & Giustino, F. Fröhlich electron-phonon vertex from first principles. *Phys. Rev. Lett.* **115**, 176401 (2015).
37. Margine, E. R. & Giustino, F. Anisotropic Migdal-Eliashberg theory using Wannier functions. *Phys. Rev. B* **87**, 024505 (2013).
38. Anderson, P. W. Theory of dirty superconductors. *J. Phys. Chem. Solids* **11**, 26 (1959).
39. Koželj, P. Discovery of a superconducting high-entropy alloy. *Phys. Rev. Lett.* **113**, 107001 (2014).
40. Guo, J. et al. Robust zero resistance in a superconducting high-entropy alloy at pressures up to 190 GPa. *Proc. Natl. Acad. Sci. USA* **114**, 13144 (2017).

41. Onen, M. et al. Nanosecond protonic programmable resistors for analog deep learning. *Science* **377**, 539 (2022).
42. Cai, M. et al. Stalling oxygen evolution in high-voltage cathodes by lanthurization. *Nat. Energy* **8**, 159–168 (2023).
43. Dong, Y., Motta, A. T. & Marquis, E. A. Atom probe tomography study of alloying element distributions in Zr alloys and their oxides. *J. Nucl. Mater.* **442**, 270 (2013).
44. Žguns, P., Gedik, N., Yildiz, B. & Li, J. Superconductivity and Pronounced Electron-Phonon Coupling in Rock-Salt Al1 − xO1 − x and Ti1 − xO1 − x. *Adv. Electronic Mater.* https://doi.org/10.1002/aelm.202400141 (2024).
45. Fan, W. et al. Anodic shock-triggered exsolution of metal nanoparticles from perovskite oxide. *J. Am. Chem. Soc.* **144**, 7657 (2022).
46. Hohenberg, P. & Kohn, W. Inhomogeneous electron gas. *Phys. Rev*. https://doi.org/10.1103/PhysRev.136.B864 (1964).
47. Kohn, W. Self-consistent equations including exchange and correlation effects. *Phys. Rev.* **140**, A1133 (1965).
48. Giannozzi, P. et al. QUANTUM ESPRESSO: a modular and open-source software project for quantum simulations of materials. *J. Phys. Condens. Matter* **21**, 395502 (2009).
49. Giannozzi, P. et al. Advanced capabilities for materials modelling with Quantum ESPRESSO. *J. Phys. Condens. Matter* **29**, 465901 (2017).
50. Perdew, J. P., Burke, K. & Ernzerhof, M. Generalized gradient approximation made simple. *Phys. Rev. Lett.* **77**, 3865 (1996).
51. Perdew, J. P. et al. Restoring the density-gradient expansion for exchange in solids and surfaces. *Phys. Rev. Lett.* **100**, 136406 (2008).
52. Blöchl, P. E. Projector augmented-wave method. *Phys. Rev. B* **50**, 17953 (1994).
53. Mostofi, A. A. Wannier90: a tool for obtaining maximally-localised Wannier functions. *Comput. Phys. Commun.* https://www.sciencedirect.com/science/article/abs/pii/S0010465507004936?via%3Dihub (2008).
54. Noffsinger, J. et al. EPW: A program for calculating the electron–phonon coupling using maximally localized Wannier functions. *Comput. Phys. Commun.* **181**, 2140 (2010).
55. Poncé, S., Margine, E. R., Verdi, C. & Giustino, F. EPW: electron–phonon coupling, transport and superconducting properties using maximally localized Wannier functions. *Comput. Phys. Commun.* **209**, 116 (2016).

Acknowledgements

The authors thank Prof. Qiang Zhu for helpful discussions. We acknowledge support by the Gordon and Betty Moore Foundation's EPiQS Initiative, Grant GBMF11945.

Author contributions

H.X. and J.L. conceived the idea and designed the project. H.X. performed the calculations. H.X., O.S., and M.P. analyzed the data. J.L. and R.J. supervised the project. H.X. wrote the manuscript with input from all authors.

Competing interests

The authors declare no competing interests.

Additional information

Supplementary information The online version contains supplementary material available at https://doi.org/10.1038/s41524-026-02040-x.

Correspondence and requests for materials should be addressed to Haowei Xu or Ju Li.

Supplementary Materials
to
Prediction of Ambient-Pressure High-Temperature Superconductivity in Electronically Modified Transition-Metal Hydrides

Haowei Xu [1,2,*], Olivia Schneble [3], Rafael Jaramillo [3],
Marek Polański [4] and Ju Li [2,3,†]

[1] Department of Physics, City University of Hong Kong, Kowloon, Hong Kong SAR, China

[2] Department of Nuclear Science and Engineering, Massachusetts Institute of Technology, Cambridge, MA 02139, USA

[3] Department of Materials Science and Engineering, Massachusetts Institute of Technology, Cambridge, MA 02139, USA

[4] Military University of Technology, 2 Kaliskiego Street, 00-908 Warsaw, Poland

Address correspondence to * haoweixu@cityu.edu.hk and † liju@mit.edu

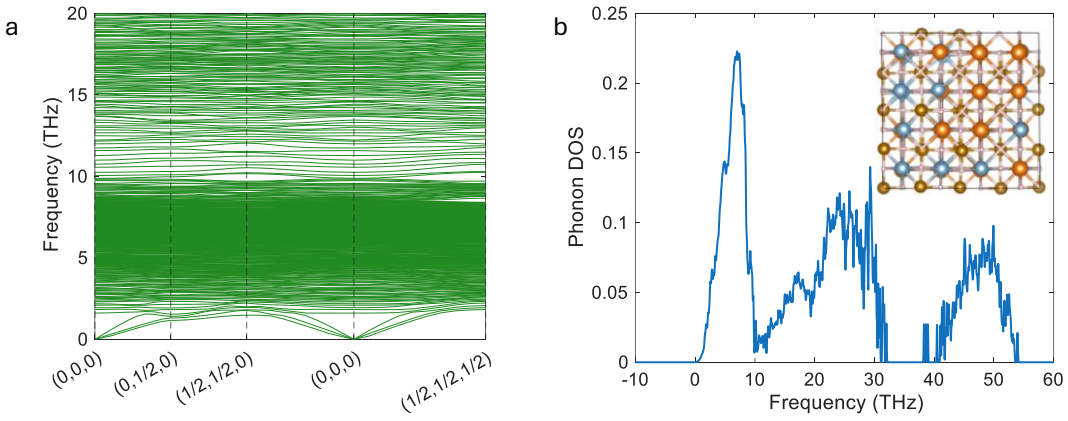

Figure S1. (a) Phonon dispersion and (b) phonon density of states of the random alloy $Mg_{32}Al_{32}Fe_{32}H_{192}$, in the unit of states per THz per formula unit. In (a), the *y*-axis is truncated at 20 THz to increase visibility at low frequencies. The inset of (b) is the atomic structure of the $Mg_{32}Al_{32}Fe_{32}H_{192}$ supercell used in the calculation.

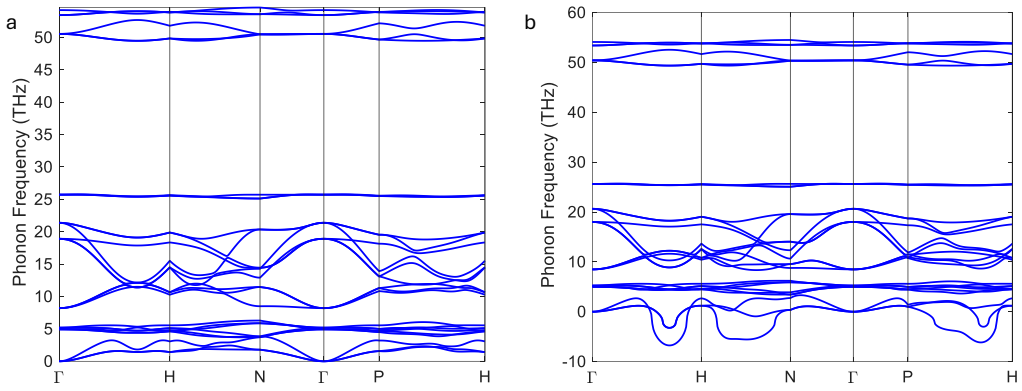

Figure S2. Phonon dispersion of $MgAlFeH_6$ with (a) $n = +0.9$ e/f. u. and (b) $n = +1$ e/f. u. hole doping concentration. Imaginary frequency phonons appear, and the structures become dynamically unstable when the hole doping concentration is $n \gtrsim +1$ e/f. u.

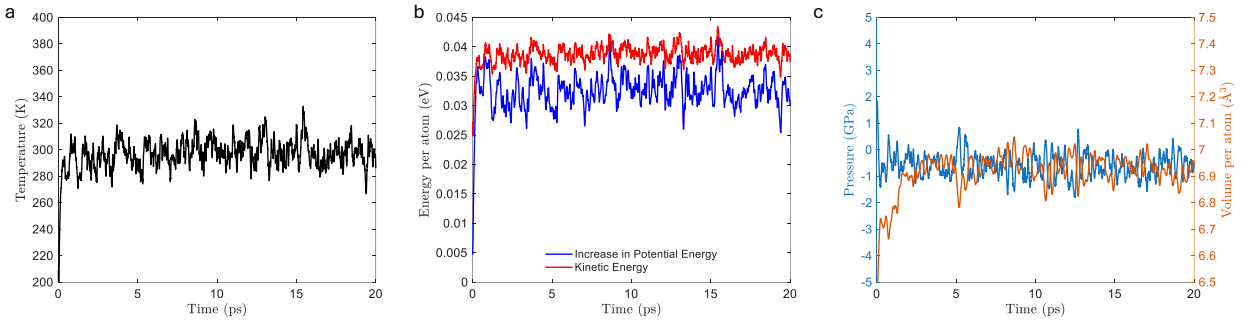

Figure S3. *Ab initio* molecular dynamics simulations for a $MgAlFeH_6$ supercell containing 288 atoms, using an NPT ensemble at 300 K and zero pressure. (a) Temperature, (b) kinetic energy and the increase in potential energy, and (c) pressure and volume are plotted as functions of time. A moving average over 50 fs was applied to reduce high-frequency oscillations. The initial structure is the fully relaxed zero-pressure, 0 K configuration, which has a relatively small volume. Upon heating to 300 K, the volume increases to approximately 7 $Å^3$ per atom.

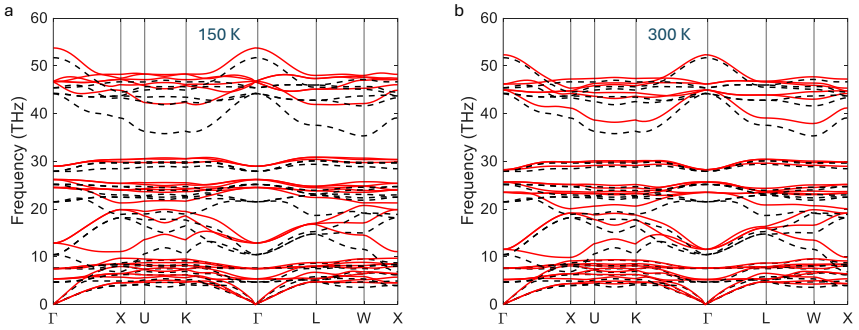

Figure S4. Phonon dispersions of $MgAlFeH_6$, including anharmonic effects, calculated using the stochastic self-consistent harmonic approximation (SSCHA) at (a) 150 K and (b) 300 K. The black dashed curves show the harmonic phonon dispersions (without anharmonicity), while the solid red curves represent the anharmonic results. The list of high-symmetry points in the Brillouin zone are listed below.

High Symmetry point	Direct Coordinate
Γ	(0,0,0)
X	$(0.5, 0, 0.5)$
U	$(0.625, 0.25, 0.625)$
K	$(0.375, 0.375, 0.75)$
L	$(0.5, 0.5, 0.5)$
W	$(0.5, 0.25, 0.75)$